

ARTICLE

Open Access

Metastable alloying structures in $\text{MAPbI}_{3-x}\text{Cl}_x$ crystals

Wen-Cheng Qiao¹, Jianming Yang², Wei Dong¹, Guang Yang¹, Qinye Bao², Rong Huang², Xue Lu Wang¹ and Ye-Feng Yao¹

Abstract

Chlorine incorporation engineering has been widely used in optoelectronic devices based on methylammonium lead iodide (MAPbI_3) perovskites. However, the characteristics of I/Cl alloying structures in $\text{MAPbI}_{3-x}\text{Cl}_x$ mixed-halide perovskites and their influences on the optoelectronic properties have been issues of a long-standing controversy. Here, we present a detailed study of the I/Cl alloying structures in $\text{MAPbI}_{3-x}\text{Cl}_x$ ($x = 0.0$ to 0.3) single crystals. We found that a small amount of Cl can substitute for the iodide of the PbI_3 inorganic lattice, leading to a phase transition from the tetragonal to cubic phase and anomalous cation dynamics evolution. Analyses based on time-dependent X-ray diffraction, ^{207}Pb NMR, and ^2H NMR indicate that the alloying structures of the $\text{MAPbI}_{3-x}\text{Cl}_x$ crystals are metastable and decompose over time. In addition, the photocurrent response measurement of $\text{MAPbI}_{3-x}\text{Cl}_x$ proved a close correlation between the alloying structures and photoelectric properties of the material. This work sheds light on the essential understanding of the I/Cl alloying structure and provides a plausible explanation for the controversy regarding the role of chloride ions in optoelectronic devices.

Introduction

The development of organic-metal halide perovskite materials with the formula ABX_3 , where A is generally either methylammonium (MA) or formamidinium (FA), B is Pb or Sn, and X is I, Br, or Cl, has rapidly progressed in recent years. These materials have been employed in a wide array of applications, such as in solar cells^{1–3}, photodetectors⁴, light-emitting diodes (LEDs)⁵, transistors⁶, and lasers⁷, owing to their excellent optoelectronic performances, such as adjustable bandgaps⁸, high absorption coefficients⁹, and long charge-carrier diffusion lengths¹⁰. The power conversion efficiencies of perovskite solar cells have significantly increased in recent years, and a high power conversion efficiency of 25.2% was obtained last

year for a solar cell based on a structurally optimized organic-metal halide perovskite¹¹. Recently, halide alloying engineering has been developed as a critically important strategy for promoting the performance of optoelectronic devices based on organic-metal halide perovskite materials¹². This strategy has been particularly applied to mixed-halide $\text{APbI}_{3-x}\text{Cl}_x$ perovskite materials^{13–16}, and progress in this area has rapidly developed. This strategy has been demonstrated to not only improve the optoelectronic properties of the resulting perovskite materials but also enhance their structural stability and even be applicable to bandgap modulation^{17,18}. However, despite this promising progress, a number of fundamental issues regarding the halide alloying engineering process remain unresolved. A particularly important issue involving how Cl atoms are incorporated into $\text{MAPbI}_{3-x}\text{Cl}_x$ materials as a halide alloying agent is a subject of strong debate^{19,20}.


On one side of the above-discussed debate, many reports have provided evidence indicating that no Cl ions are embedded in the inorganic PbI_3 lattice. This suggests

Correspondence: Xue Lu Wang (xlwang@phy.ecnu.edu.cn) or Ye-Feng Yao (yfyao@phy.ecnu.edu.cn)

¹Physics Department & Shanghai Key Laboratory of Magnetic Resonance, School of Physics and Electronic Science, East China Normal University, North Zhongshan Road 3663, 200062 Shanghai, People's Republic of China

²Key Laboratory of Polar Materials and Devices, Department of Electronic Sciences, School of Physics and Electronic Sciences, East China Normal University, 200241 Shanghai, People's Republic of China

© The Author(s) 2020

 **Open Access** This article is licensed under a Creative Commons Attribution 4.0 International License, which permits use, sharing, adaptation, distribution and reproduction in any medium or format, as long as you give appropriate credit to the original author(s) and the source, provide a link to the Creative Commons license, and indicate if changes were made. The images or other third party material in this article are included in the article's Creative Commons license, unless indicated otherwise in a credit line to the material. If material is not included in the article's Creative Commons license and your intended use is not permitted by statutory regulation or exceeds the permitted use, you will need to obtain permission directly from the copyright holder. To view a copy of this license, visit <http://creativecommons.org/licenses/by/4.0/>.

that Cl ions influence the optoelectronic properties of $\text{MAPbI}_{3-x}\text{Cl}_x$ perovskites only in an indirect way, and numerous indirect enhancement effects have been proposed. For example, Chen et al.¹⁹ attributed the optoelectronic performance enhancement of $\text{MAPbI}_{3-x}\text{Cl}_x$ perovskites to the improved heterojunction interfaces induced by the Cl ion incorporation process. Lian et al.²⁰ demonstrated that Cl ion incorporation could improve the crystallinity of $\text{MAPbI}_{3-x}\text{Cl}_x$ perovskite materials and in turn increase the crystal growth rate. However, no Cl ions were detected in the crystal lattice. Fan et al.²¹ proposed that residual PbCl_2 passivated defects in $\text{MAPbI}_{3-x}\text{Cl}_x$ perovskite thin films and thereby improved their electrical properties. On the other side of the debate, a similar number of reports have provided evidence that Cl ions can be embedded in the inorganic PbI_3 lattice. For example, Zhang et al.²² demonstrated the presence of Cl ions in the inorganic lattice of $\text{MAPbI}_{3-x}\text{Cl}_x$ nanofibers fabricated using a solution-assembly method. Zhang et al.²³ reported that Cl can be maximally doped into the $\text{MAPbI}_{3-x}\text{Cl}_x$ perovskite crystal lattice using an ion exchange–decomposition process. Min et al.²⁴ demonstrated that Cl ions can be introduced into the FAPbI_3 crystal lattice through the substitution of FA sites with methylenediammonium dichloride ions. In addition, the possible crystal structures of $\text{MAPbI}_{3-x}\text{Cl}_x$ perovskite materials have been investigated by ab initio computer simulation studies, and the potential optoelectronic properties of the proposed structures have been evaluated^{25,26}. However, previous studies mainly focused on perovskite films, whose lack of stability and the difficult distinction between the surface and bulk are great challenges for accurate detection by various instruments. Moreover, few studies have rigorously examined the I/Cl alloying structures and their long-term stability.

The present study seeks to address this long-standing controversy by presenting a detailed study of the I/Cl alloying structures observed in a series of $\text{MAPbI}_{3-x}\text{Cl}_x$ ($x = 0, 0.05, 0.1, 0.3, 0.4,$ and 0.5) single crystal perovskite samples over time. Here, single-crystal samples are much more ideal than powder samples for the proposed study owing to their greatly reduced crystal defect concentrations and fewer crystal boundaries^{10,20}. The structure of the single crystals is observed to change from tetragonal to cubic with increasing x . Characterization of the samples by means of X-ray diffraction (XRD), X-ray photoelectron spectroscopy (XPS), ²⁰⁷Pb nuclear magnetic resonance (NMR), and ²H NMR reveals that a small amount of Cl can be incorporated into the iodide sites of the inorganic PbI_3 lattice, leading to a phase transition from the tetragonal to cubic phase and a series of anomalous cation dynamics evolutions including a slower rotation rate and a more disordered dynamics tendency. Analyses based on time-dependent XRD, ²⁰⁷Pb NMR, and

²H NMR indicate that the I/Cl alloying structures of the $\text{MAPbI}_{3-x}\text{Cl}_x$ crystals are metastable and disappear over time at room temperature. In addition, we explored the photoelectric properties of $\text{MAPbI}_{3-x}\text{Cl}_x$ single-crystal photodetectors and found that the photocurrent response obviously decreases over time, even though Cl incorporation helps boost the photocurrent response. This long-term instability indicates that different conclusions regarding the effect of Cl ions on the properties of $\text{MAPbI}_{3-x}\text{Cl}_x$ perovskites may arise over different time scales, which provides a plausible explanation for the long-standing controversy regarding the effect of Cl ions on the performance of optoelectronic devices based on $\text{MAPbI}_{3-x}\text{Cl}_x$.

Materials and methods

Materials

All reagents were used as received without further purification: PbI_2 (99.999%, Sigma-Aldrich), methylamine hydroiodide (MAI, 99.5%, Xi'an Polymer Light Technology Corp), methylamine hydrochloride (MACl, 99.5%, Xi'an Polymer Light Technology Corp), methylamine hydrobromide (MABr, 99.5%, Xi'an Polymer Light Technology Corp), deuterated methylamine hydroiodide ($\text{CD}_3\text{NH}_3\text{I}$, 99%, Cambridge Isotope Laboratories Inc), deuterated methylamine hydroiodide (MACl, 99.5%, Cambridge Isotope Laboratories Inc), gamma-butyrolactone (GBL, 99.99%, Sigma-Aldrich), dimethylformamide (DMF, 99.99%, Sigma-Aldrich), and dimethylsulfoxide (DMSO, 99.99%, Sigma-Aldrich).

Crystallization of $\text{CH}_3\text{NH}_3\text{PbI}_{3-x}\text{Cl}_x/\text{CD}_3\text{NH}_3\text{PbI}_{3-x}\text{Cl}_x$ single crystals

MAI, MACl, and PbI_2 were mixed and dissolved at different molar ratios into GBL as the precursor solution. DMF was chosen as the second solvent when the concentration of MACl exceeded 0.2 M because of the low solubility of MACl in GBL. During dissolution, the precursor solution was ultrasonicated and heated to 60 °C. Next, a filter (0.2 μm) was used to filter invisible impurities. After the above solution was heated and kept at 110 °C for 12 h, $\text{MAPbI}_{3-x}\text{Cl}_x$ single crystals were harvested. The X-ray 2θ scan on the maximal facet of the typical $\text{MAPbI}_{3-x}\text{Cl}_x$ single crystals showed two sharp diffraction peaks, suggesting a well-structured single-crystalline nature (Supplementary Fig. S1). Deuterated $\text{MAPbI}_{3-x}\text{Cl}_x$ was synthesized using a similar approach to that mentioned above, except that $\text{CD}_3\text{NH}_3\text{I}$ and $\text{CD}_3\text{NH}_3\text{Cl}$ were used as cation sources.

It is noteworthy that the crystals could be obtained by the above method only for $x \leq 0.5$. For $x > 0.5$, no crystal was synthesized. However, we found that a new trace MAPbCl_3 phase grew together with the double halogen perovskite component when x was above 0.3, as proven by

the XRD pattern in Supplementary Fig. S2 and ^{207}Pb NMR spectrum in Supplementary Fig. S3. As a result, this article focuses only on the samples with $x \leq 0.3$.

Crystallization of $\text{MAPbI}_{3-x}\text{Br}_x$ single crystals

$\text{CH}_3\text{NH}_3\text{I}$, $\text{CH}_3\text{NH}_3\text{Br}$, and PbI_2 were mixed and dissolved at different molar ratios into GBL as the precursor solution, and a filter (0.2 μm) was used to filter invisible impurities. After the above solution was heated and kept at 100 $^\circ\text{C}$ for 12 h, $\text{MAPbI}_{3-x}\text{Br}_x$ single crystals were harvested. The static ^{207}Pb NMR spectra of the $\text{MAPbI}_{3-x}\text{Br}_x$ ($x = 0, 0.2, 1, 3$) samples are shown in Supplementary Fig. S4.

Crystallization of MAPbBr_3 and $\text{MAPbCl}_3/\text{CD}_3\text{NH}_3\text{PbI}_3$ single crystals

To grow perovskite $\text{CH}_3\text{NH}_3\text{PbBr}_3$ single crystals, MABr and PbBr_2 (1:1) were mixed and dissolved in DMF, with the concentration controlled at 1.0 M. A filter (0.2 μm) was used to filter invisible impurities. After the above solution was heated and kept at 80 $^\circ\text{C}$ for 6 h, MAPbBr_3 single crystals were harvested. To grow the single-crystalline perovskite $\text{CH}_3\text{NH}_3\text{PbCl}_3$, MACl , and PbCl_2 (1:1) were mixed and dissolved in a mixed solution of DMSO and DMF (1:1), with the concentration controlled at 2.0 M. A filter (0.2 μm) was used to filter invisible impurities. After the above solution was heated and kept at 80 $^\circ\text{C}$ for 6 h, MAPbCl_3 single crystals were harvested. Deuterated MAPbI_3 was synthesized using a similar approach to that mentioned above except that $\text{CD}_3\text{NH}_3\text{I}$ and $\text{CD}_3\text{NH}_3\text{I}$ were used as cation sources.

Powder X-ray diffraction (XRD) patterns

XRD measurements were carried out on a Rigaku Smart Lab (X-ray source: Cu K α ; $\lambda = 1.54186 \text{ \AA}$) operated at 40 kV and 30 mA. $\text{MAPbI}_{3-x}\text{Cl}_x$ powders were made by grinding a large piece of crystal into a fine powder.

XPS spectra

XPS spectra were measured by an X-ray photoelectron spectrometer (PHI Quantro SXM, ULVAC-PHI) with an Ar ion gun sputtering the surface. Before measuring the sample, the crystal surface was polished in a glove box filled with inert nitrogen gas to expose a fresh surface.

Static ^{207}Pb solid-state NMR

^{207}Pb NMR experiments were carried out on a 300 M NMR instrument operating at 62.73 MHz for ^{207}Pb . A Bruker two-channel static PE probe with a homemade 4 mm coil was used to record the spectra. The ^{207}Pb spectra were acquired using a single pulse excitation pulse sequence. The excitation pulse in the experiments was 2.5 μs at an RF field strength of 100 kHz. The recycle delay was 1 s. All ^{207}Pb NMR spectra were referenced to

PbMe_4 ($\delta(^{207}\text{Pb}) = 0 \text{ ppm}$) by setting the ^{207}Pb peak of nonspinning solid MAPbCl_3 measured at 293 K to -647.5 ppm .

^1H solid-state MAS NMR

^1H NMR spectra were recorded with a 600 M NMR instrument operating at 600.44 MHz. The spinning rate was set to 10 kHz. The recycle delay was set to 2 s. All ^1H chemical shifts were calibrated using adamantane ($\delta = 1.85 \text{ ppm}$).

Static ^2H solid-state NMR

^2H NMR experiments were carried out on a 300 M NMR instrument operating at 46.07 MHz for ^2H . A Bruker two-channel static PE probe with a homemade 4 mm coil was used to record the spectra. The ^2H spectra were acquired using the solid echo sequence. The ^2H pulse width was 2.5 μs at an RF field strength of 100 kHz. The ^2H patterns were simulated via the weblab (<http://weblab.mpip-mainz.mpg.de/weblab/>).

Results and discussion

Preparation and characterization of $\text{MAPbI}_{3-x}\text{Cl}_x$ single crystals

The materials and methods employed for preparing the $\text{MAPbI}_{3-x}\text{Cl}_x$ single crystal samples used in the present study are outlined in detail in the Materials and Methods. The preparation procedures are briefly described as follows. The inverse temperature crystallization (ITC) method was used to prepare MAPbI_3 (i.e., $x = 0$) single crystal perovskites^{27,28}. For $\text{MAPbI}_{3-x}\text{Cl}_x$ single crystal samples, x was varied by adjusting the proportions of methylamine hydrochloride (MACl) and methylamine hydroiodide (MAI) employed during synthesis while retaining a constant concentration of PbI_2 . Here, MACl was first added into a pure gamma-butyrolactone (GBL) solvent. However, this often yielded a turbid solution due to the poor solubility of MA in GBL, as shown in Fig. 1A. Nonetheless, the solution became transparent again once MAI and PbI_2 were added, as shown in Fig. 1B. Second, the solution was heated to 383 K to promote the growth of single crystals. Representative single-crystal $\text{MAPbI}_{3-x}\text{Cl}_x$ samples are shown in Fig. 1C and Supplementary Fig. S1 against a cm^2 square inscribed background to indicate the sample sizes. We note that MAPbCl_3 impurity phases are synthesized together with $\text{MAPbI}_{3-x}\text{Cl}_x$ crystals for $x > 0.3$ (Supplementary Figs. S2 and S3). Hence, $x = 0.3$ was the largest value considered in the present study. Notably, reflecting the influence of Cl^- doping on the crystal structure, the shapes of the single crystal samples change with increasing Cl^- concentration. The changes in the crystal shape do not indicate a change in the crystal symmetry or the formation of a polycrystalline component. Similar phenomena have been observed in MAPbI_3 single crystals²⁹.

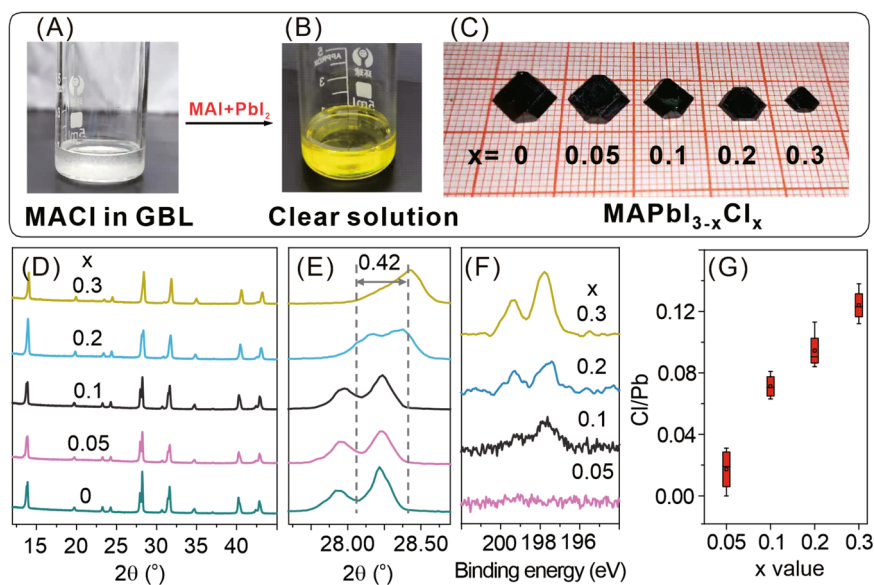


Fig. 1 Precursor solution growth process and structural characterization of $\text{MAPbI}_{3-x}\text{Cl}_x$ single crystal samples ($x = 0, 0.05, 0.1, 0.2$, and 0.3). **A** Undissolved MAI in a GBL solution; **B** MAI solids completely dissolved in a GBL solution after adding MAI and PbI_2 ; **C** photos of single-crystal samples; **D** XRD patterns of the samples in powder form; **E** enlarged XRD patterns from **D**, **E** showing the (004) and (220) diffraction peaks; **F** XPS Cl $2p$ core-level spectra; **G** Cl/Pb atomic ratios obtained from XPS results with respect to x .

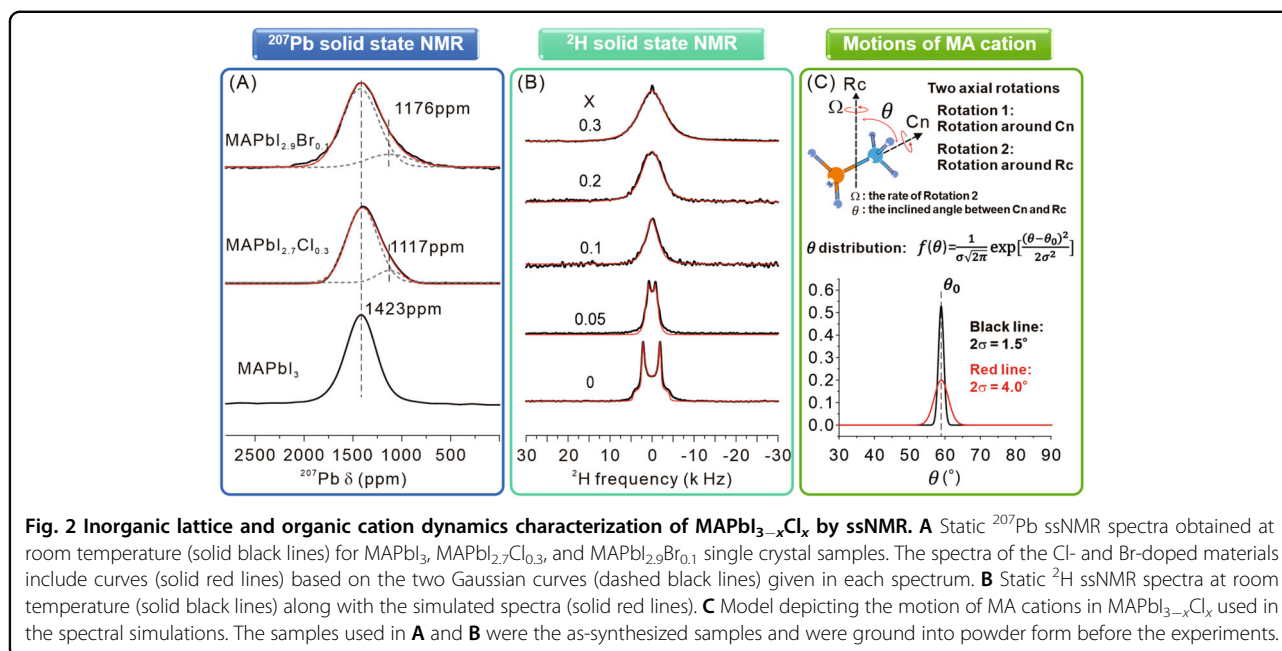
Figure 1D, E presents the XRD patterns and enlarged views of the patterns in the 2θ range from ~ 28 to 29° , respectively, for $\text{MAPbI}_{3-x}\text{Cl}_x$ ($x = 0, 0.05, 0.1$, and 0.3) single crystal samples at room temperature. We note the presence of a clear splitting of the two peaks indicative of the (004) and (220) facets of the MAPbI_3 sample at 2θ values ranging from 28 to 29° . This is a characteristic feature of the diffraction peaks obtained for MAPbI_3 perovskite single crystals in the tetragonal phase at room temperature³⁰. These (220) and (004) peaks are observed to shift gradually toward increasing 2θ values with increasing x in the range of 0.05 – 0.3 . This gradual shift indicates that Cl doping causes the dimensions of the crystal lattice cell to progressively decrease with increasing x . We also note that the (220) and (004) diffraction peaks gradually merge with increasing x , indicating that the $\text{MAPbI}_{3-x}\text{Cl}_x$ single crystal lattice structure gradually changes from the tetragonal phase to the cubic phase with increasing x , as verified in past studies³¹.

The atomic concentrations of Cl atoms in the $\text{MAPbI}_{3-x}\text{Cl}_x$ single crystal samples were evaluated using high-resolution XPS. Prior to conducting XPS analysis, the surface of each single crystal sample was mechanically polished to avoid the influence of residual solvent on the XPS results. Figure 1F presents the XPS Cl $2p$ core-level spectra of the Cl atoms in the samples, which are composed of the Cl $2p_{1/2}$ and Cl $2p_{3/2}$ doublet states. We note that the Cl $2p$ signal intensity clearly increases with increasing x . The atomic Cl concentrations in the samples were determined relative to the atomic Pb concentrations

from the areas under the Cl $2p$ and Pb $4f$ curves of the XPS core-level spectra obtained at multiple points of each sample surface and scaled according to their respective sensitivity factors. According to the chemical formula $\text{MAPbI}_{3-x}\text{Cl}_x$, the atomic ratio of Pb/Cl should be equal to x . The Cl/Pb atomic ratios obtained through four repeated tests on the same batch of samples are plotted in Fig. 1G with respect to x . Clearly, the Cl/Pb atomic ratio increases with increasing x , as expected. However, the Cl/Pb atomic ratio in the samples does not scale according to x , and only a Cl/Pb atomic ratio of 0.138 ± 0.021 is obtained for $x = 0.3$, which is much less than the expected value. This indicates that a substantial proportion of Cl ions failed to enter the single crystal and were accumulated in the precursor during crystal growth, further inhibiting crystal growth. The results also explain why the sample size decreases with increasing x (Fig. 1C).

Static solid-state ^{207}Pb and ^2H NMR characterization of $\text{MAPbI}_{3-x}\text{Cl}_x$ materials

Figure 2A presents the ^{207}Pb solid-state NMR (ssNMR) spectra (solid black lines) of MAPbI_3 and $\text{MAPbI}_{2.7}\text{Cl}_{0.3}$ single crystal samples. The ^{207}Pb ssNMR results reveal clear changes in the local Pb environments with increasing x . As the central atom in the PbX_6 octahedra, the changes in the local environment of Pb can be associated with variations in the chemical bonds between Pb and the surrounding halogen atoms. For comparison, the ^{207}Pb ssNMR spectrum of a $\text{MAPbI}_{2.9}\text{Br}_{0.1}$ single crystal sample, synthesized by the same procedure as $\text{MAPbI}_{3-x}\text{Cl}_x$, is

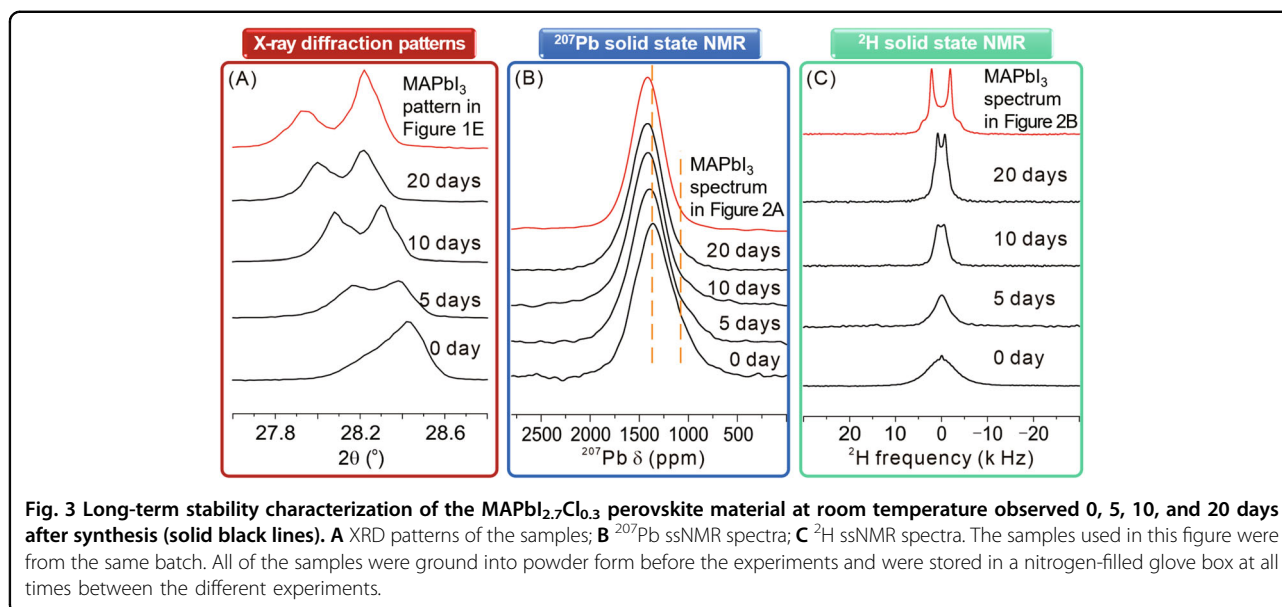


also given in Fig. 2A. The spectra of the Cl- and Br-doped materials include curves (solid red lines) based on the two Gaussian curves (dashed black lines) given in each spectrum. The ²⁰⁷Pb ssNMR spectrum of the MAPbI₃ crystal sample presents a very broad symmetrical peak with a chemical shift (δ) of 1423 ppm. In contrast, the spectrum of the MAPbI_{2.7}Cl_{0.3} sample has a main peak consistent with that of the MAPbI₃ spectrum, and a clear shoulder peak is observed at 1117 ppm. The origin of this shoulder peak can be assigned based on a comparison with the shoulder peak in the ²⁰⁷Pb ssNMR spectrum observed for the MAPbI_{2.9}Br_{0.1} single crystal sample at 1176 ppm, which was assigned to a PbI₅Br alloying structure in a past study^{32,33}. Here, the PbI₅Br alloying structure includes five iodine atoms and one bromine atom connected to a Pb atom to form an octahedron. We thus tentatively assign the shoulder peak of the MAPbI_{2.7}Cl_{0.3} spectrum to the PbI₅Cl unit. If this assignment is valid, then it would indicate that Cl atoms can replace I atoms in the crystal lattice in a manner similar to that observed in the MAPbI_{2.9}Br_{0.1} crystal. Details regarding the ²⁰⁷Pb ssNMR spectrum analysis are outlined in Section S2, in conjunction with Supplementary Figs. S4–6.

An alternative method of detecting changes in the lattice structure of MAPbI₃ perovskite materials is to probe the dynamic changes in the MA cations embedded in the inorganic lattice by means of ²H NMR analysis³⁴. This approach relies on the strong coupling between the MA cations and the surrounding crystal lattice³⁵. Here, small changes in the inorganic lattice cell have been reported to induce significant changes in the dynamics of the embedded MA cations^{26,36}. For this purpose,

MAPbI_{3-x}Cl_x ($x = 0, 0.05, 0.1, 0.2,$ and 0.3) samples were synthesized in which the methyl group was fully deuterated (Supplementary Fig. S7). In addition, powder samples were used in the ²H NMR experiments to ensure an adequate signal. Figure 2B presents the solid-state ²H NMR spectra (solid black lines) of the deuterated samples. The figure also includes spectra (solid red lines) simulated according to a method discussed later. For MAPbI₃, the ²H pattern exhibits a typical Pake doublet lineshape, and the lineshapes of the signals vary significantly with increasing x , indicating gradual changes in the dynamics of the MA cations in the samples, which, as discussed, can be ascribed to changes in the inorganic lattice cell environment of the MA cations.

The motion of MA cations in organic-metal halide perovskite crystals has been studied by several groups^{34,37,38}. These past studies have demonstrated that details regarding the dynamic changes in the MA cations in these perovskite samples can be obtained by analyzing the lineshapes of ²H NMR spectra. Therefore, we applied the MA cation motion model proposed by Franssen et al.³⁷ to model the motion of MA cations in the MAPbI_{3-x}Cl_x samples based on the lineshapes presented in Fig. 2B. Details regarding the lineshape analysis are outlined in section S3, in conjunction with Supplementary Figs. S8–11 and Supplementary Table S1. This process is illustrated here in Fig. 2C and described briefly as follows. An MA cation in the tetragonal phase of MAPbI₃ can undergo rotation about two axes, including intrinsic axial rotation (rotation 1) about the C_n axis along with the C–N bond formed between the CH₃ and NH₃ components of the MA cation and secondary axial rotation



(rotation 2) at a rate Ω about the Rc axis, which lies at a specific angle θ with respect to the Cn axis. The θ values are assumed to be distributed about a mean value θ_0 according to a Gaussian distribution with standard deviation σ , as indicated by the equation and graph in Fig. 2C. Applying this model with $2\sigma = 1.5^\circ$ to the ²H spectrum obtained for the MAPbI₃ sample in Fig. 2B yields a θ_0 of 58.9°, and the difference between the doublet peaks of the Pake lineshape (ν_{QS}) is 4 kHz. We note that the simulated ²H NMR spectrum is in good agreement with the actual spectrum. For MAPbI_{2.95}Cl_{0.05}, the observed ²H NMR spectrum lineshape undergoes obvious changes, where the separation between the two peaks of the Pake doublet lineshape decreases significantly. Applying the model with $2\sigma = 1.5^\circ$ to the ²H spectrum MAPbI_{2.95}Cl_{0.05} yields a θ_0 of 57.5°. The slight reduction in θ_0 with increasing x stems from the slight phase transition tendency from the tetragonal phase to the cubic phase revealed by XRD in Fig. 1E. With a further increase in x , we note that the ²H patterns gradually transform into a single broad peak for MAPbI_{3-x}Cl_x ($x = 0.1, 0.2,$ and 0.3). The lineshape analysis results indicate that the appearance of a broad peak can be attributed to a decrease in Ω , accompanied by an increase in σ . Based on the strong coupling between the MA cations and the inorganic lattice, we can conclude that these changes in the motion of MA cations are associated with the lattice contraction and lattice distortion caused by the random and partial substitution of iodine ions with Cl ions in the inorganic lattice. We also note that compared with the XRD and ²⁰⁷Pb NMR results, the ²H NMR spectra appear to exhibit a much greater sensitivity to structural changes in the inorganic framework, indicating the great potential

of this technique for probing structural changes in MAPbI₃ perovskite materials.

Time-dependent structural characterization of MAPbI_{3-x}Cl_x materials

Figure 3A presents the time-dependent XRD patterns (solid black lines) of the MAPbI_{2.7}Cl_{0.3} single crystal sample obtained over a 2θ range of 27.6° to 28.8° at 0, 5, 10, and 20 days after synthesis. The samples were stored in a nitrogen-filled glove box between measurements to eliminate the influence of water vapor and oxygen as much as possible. The solid red line in the figure corresponds to the XRD pattern of the MAPbI₃ single crystal sample originally shown in Fig. 1E. In comparison with the XRD pattern of the MAPbI₃ single crystal sample, we note that the XRD pattern of the originally cubic MAPbI_{2.7}Cl_{0.3} single-crystal shown in Fig. 3A gradually transitions over the 20-day period to an XRD pattern very similar to that observed for the MAPbI₃ single crystal sample with a tetragonal structure. This strongly indicates that the MAPbI_{2.7}Cl_{0.3} crystal underwent a gradual solid-phase transition from the cubic phase to the tetragonal phase.

Figure 3B presents the time-dependent ²⁰⁷Pb NMR results obtained for the MAPbI_{2.7}Cl_{0.3} single crystal sample at 0, 5, 10, and 20 days after synthesis. As before, the samples were stored in a nitrogen-filled glove box at all times between testing. The solid red line in the figure corresponds to the ²⁰⁷Pb NMR spectrum of the MAPbI₃ single crystal sample originally shown in Fig. 2A. In comparison with the ²⁰⁷Pb NMR spectrum of the MAPbI₃ single crystal sample, we note that the ²⁰⁷Pb NMR spectrum of the MAPbI_{2.7}Cl_{0.3} single-crystal shown in Fig. 3B

gradually transitions over the 20-day period to a symmetrical ^{207}Pb NMR spectrum very similar to that observed for the MAPbI_3 single crystal sample, with equivalent peak shifts of 1423 ppm. Here, the shoulder observed in the as-synthesized sample was greatly diminished after 5 days and completely disappeared after 10 days. As discussed above, the shift in the main peak and the appearance of the shoulder can be related to the formation of PbI_5Cl alloying structures. Accordingly, the reverse shift of the main peaks and the disappearance of the shoulder thus strongly indicate that the PbI_5Cl alloying structures gradually changed and disappeared over time.

Figure 3C presents the time-dependent ^2H NMR results obtained for the deuterated $\text{MAPbI}_{2.7}\text{Cl}_{0.3}$ powder sample at 0, 5, 10, and 20 days after synthesis. As before, the samples were stored in a nitrogen-filled glove box at all times between testing. The solid red line in the figure corresponds to the ^2H NMR spectrum of the MAPbI_3 deuterated powder sample originally shown in Fig. 2B. In comparison with the ^2H NMR spectrum of the MAPbI_3 sample, we note that the ^2H NMR spectrum of the $\text{MAPbI}_{2.7}\text{Cl}_{0.3}$ single-crystal shown in Fig. 3C gradually transitions over the 20-day period to a standard Pake doublet lineshape similar to that observed for the MAPbI_3 single crystal sample. Here, the broad peak observed in the as-synthesized sample became considerably less broad after 5 days, and Pake doublet peaks began to emerge after 10 days. However, we note that the lineshape of the ^2H NMR spectrum acquired after 20 days failed to fully return to that of the MAPbI_3 spectrum, indicating that some residual distortion remains in the inorganic lattice of the sample.

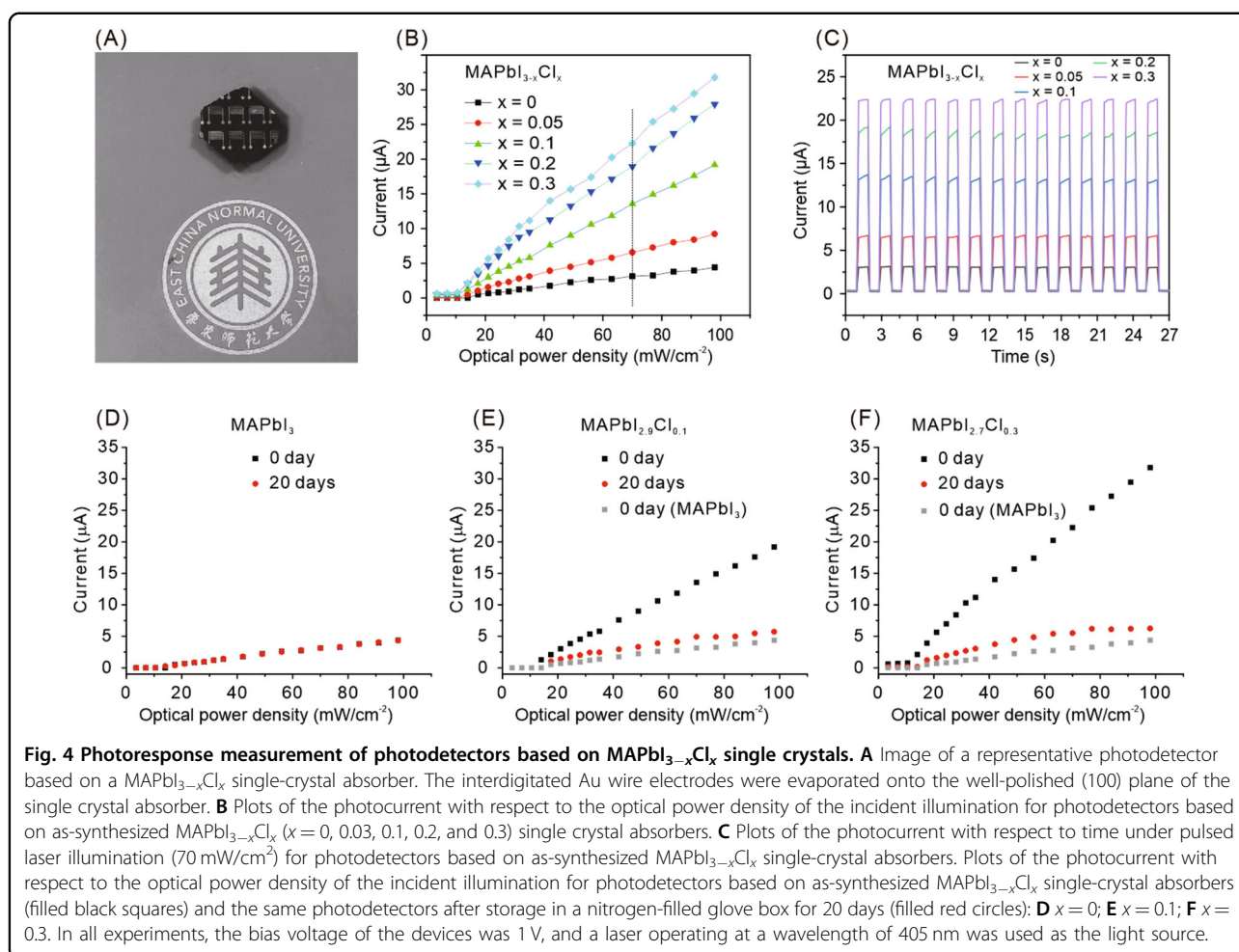
The ^2H NMR spectra of the as-synthesized $\text{MAPbI}_{2.7}\text{Cl}_{0.3}$ sample were also acquired at different temperatures (i.e., 294, 310, 330, and 340 K; see Supplementary Fig. S12 in Supporting Information). It was observed that the lineshapes of the ^2H NMR spectra remained nearly unchanged before and even after exceeding the phase transition temperature of MAPbI_3 (337 K). This result indicates that the $\text{MAPbI}_{2.7}\text{Cl}_{0.3}$ structure does not undergo a similar phase transition as that of MAPbI_3 . This may also be associated with the doping of Cl atoms in the inorganic lattice.

The combined observations above clearly reveal many intriguing details regarding the structural transformations of $\text{MAPbI}_{2.7}\text{Cl}_{0.3}$ over time. As discussed, the time-dependent XRD results indicate that the $\text{MAPbI}_{2.7}\text{Cl}_{0.3}$ crystal undergoes a gradual solid-phase transition from the cubic phase to the tetragonal phase within 20 days. In addition, while the time-dependent changes in the chemical shift and lineshape of the ^{207}Pb spectrum strongly indicate that the PbI_5Cl alloying structures present in the as-synthesized sample gradually disappear over time, the ^{207}Pb NMR results cannot reveal whether the PbI_5Cl

alloying structures have completely disappeared after 20 days due to the limited sensitivity of ^{207}Pb NMR signals. The time-dependent XRD results suffer from a similar limitation in that XRD is not sensitive to local changes in the crystalline structure. Fortunately, this issue is clarified to some extent by the fact that the lineshape of the ^2H NMR spectrum acquired after 20 days did not return fully to that of the MAPbI_3 spectrum. As discussed, this indicates that some residual distortion remained in the inorganic lattice of the sample. Accordingly, this suggests that some amount of alloying structures remains in the sample but not at a sufficiently high level to sustain the cubic phase of the crystal or to greatly affect the local Pb environment overall. Clearly, ^2H NMR represents a more sensitive technique for probing changes in the inorganic lattice of MAPb_3 halide perovskite crystals due to Cl doping.

Photoresponse of photodetectors based on $\text{MAPbI}_{3-x}\text{Cl}_x$ single-crystal absorbers

The influence of Cl doping on the optoelectronic properties of $\text{MAPbI}_{3-x}\text{Cl}_x$ materials was illustrated by fabricating five planar-type photodetectors with appropriately shaped and finished $\text{MAPbI}_{3-x}\text{Cl}_x$ ($x = 0, 0.05, 0.1, 0.2,$ and 0.3) single crystal absorbers. An image of a representative photodetector device is shown in Fig. 4A. Here, interdigitated Au wire electrodes (0.5 mm in length, 40 μm in width, and approximately 100 nm thick) were evaporated on the well-polished (100) plane of each single crystal. The effective absorber area of each detector was 0.1 mm^2 . The current responses were measured under a bias voltage of 1 V with illumination provided by a 405 nm wavelength continuous laser beam with an optical power density of 0 to 100 mW/cm^2 . Figure 4B shows the photocurrent responses of the photodetectors employing the as-synthesized single-crystal absorbers as a function of the incident light intensity. The results demonstrate that the photocurrent increased almost linearly with increasing incident light intensity for each single crystal photodetector. Meanwhile, the photocurrent of the photodetectors at a given incident light intensity was positively correlated with the Cl doping ratio (i.e., x), where the photocurrent increased with increasing x . Figure 4C presents the photocurrents of the devices obtained with respect to time under continuous laser illumination operating with an optical power density of 70 mW/cm^2 . As anticipated, all of the photodetectors exhibited a very good photoresponse, where the photocurrent immediately increased and decreased at the beginning and end of each laser pulse, respectively. We also note that the photocurrent obtained at each laser pulse noticeably increased with increasing x . For example, the photocurrent of the device based on MAPbI_3 was only 3 μA , whereas that of the device based on $\text{MAPbI}_{2.7}\text{Cl}_{0.3}$ was 23 μA .



However, a comparison of the photocurrents with respect to the optical power density of the incident illumination for photodetectors based on the as-synthesized MAPbI_3 , $\text{MAPbI}_{2.95}\text{Cl}_{0.05}$, and $\text{MAPbI}_{2.7}\text{Cl}_{0.3}$ single-crystal absorbers, shown by the filled black squares in Fig. 4D, E, and F, respectively, and the same photodetectors after storage in a nitrogen-filled glove box for 20 days (filled red circles) demonstrates that the optoelectronic properties of the Cl-doped perovskite materials were not stable and degraded after 20 days of storage to photocurrents essentially commensurate with that of MAPbI_3 . The photoresponse data obtained for photodetectors based on $\text{MAPbI}_{2.9}\text{Cl}_{0.1}$ and $\text{MAPbI}_{2.8}\text{Cl}_{0.2}$ behaved similarly (Supplementary Fig. S13). In contrast, the photoresponse data obtained for the MAPbI_3 -based photodetector exhibited no obvious changes after storage for 20 days, which demonstrates the stability of the MAPbI_3 structure. The above results support the previous time-dependent analyses based on XRD, ^{207}Pb NMR, and ^2H NMR, which demonstrated that the crystal lattices of the $\text{MAPbI}_{3-x}\text{Cl}_x$ ($x = 0.05, 0.1, 0.2,$ and 0.3) single crystals changed from cubic to tetragonal after 20 days, and

the Cl alloying structures in the Cl-doped materials gradually disappeared.

As discussed, the roles of Cl ions in $\text{MAPbI}_{3-x}\text{Cl}_x$ perovskites are a very controversial issue. A number of theoretical studies have demonstrated that the substitution of Cl for I in the inorganic lattice can have an inherently positive effect on the electronic properties of $\text{MAPbI}_{3-x}\text{Cl}_x$ perovskites by reducing electron–phonon coupling and electron–hole recombination²⁵, enhancing the intensity of the p orbital of I ions in the HOMO state³⁹, or enhancing electron localization and the charge–carrier diffusion length²⁶. However, other studies have demonstrated that Cl substitution may have a negative effect on the properties of $\text{MAPbI}_{3-x}\text{Cl}_x$ perovskites^{19,22}. For example, the disassociation of Cl atoms from the inorganic lattice can generate a large amount of anionic defects in the lattice, which serve as deep-level defects that may strongly hinder the generation and diffusion of charge carriers⁴⁰. Here, the long-term instability of $\text{MAPbI}_{3-x}\text{Cl}_x$ alloying structures reported in the present work sheds some light on this controversial issue. In the as-synthesized state of

MAPbI_{3-x}Cl_x single crystals, the substitution of Cl for I contributes to enhanced electronic properties of the Cl-doped perovskites and explains the origin of their enhanced optoelectronic properties. Meanwhile, the Cl atoms gradually dissociate from the inorganic lattice over time and may result in the generation of anionic vacancies in the lattice. As a result, the optoelectronic properties of the MAPbI_{3-x}Cl_x single crystals deteriorate over time. This long-term instability indicates that different conclusions regarding the effect of Cl ions on the optoelectronic properties of MAPbI_{3-x}Cl_x perovskites may arise over different time scales, which provides a plausible explanation for the long-standing controversy regarding the effect of Cl ions on the performance of optoelectronic devices based on MAPbI_{3-x}Cl_x.

In addition, the stability issues of mixed-halide perovskites, particularly APbI_{3-x}Br_x materials, have attracted some attention recently^{41,42}. The results revealed that APbI_{3-x}Br_x can reversibly segregate into I-rich and Br-rich domains under continuous visible illumination^{43,44}. For MAPb_{3-x}Cl_x, new Cl-rich domains, such as MAPbCl₃, were not discovered in either the XRD patterns or the ²⁰⁷Pb NMR spectra. We thus hesitate to directly correlate the instability of MAPb_{3-x}Cl_x over time to the halide segregation present in APbI_{3-x}Br_x. However, the halide segregation phenomenon is possibly related to some metastable states present only under illumination. Therefore, an in situ study of MAPb_{3-x}Cl_x is worth investigating if one wants to probe the halide segregation phenomenon. Such an in situ study is ongoing in our laboratory.

Conclusion

In this article, we report a detailed study of MAPbI_{3-x}Cl_x ($x = 0.0$ to 0.3) single crystal structures based on a combination of XRD, XPS, and solid-state NMR. The results revealed that a small amount of Cl atoms could substitute for iodide atoms in the inorganic lattice of Cl-doped crystals. This substitution distorted the inorganic lattice, resulting in a transformation from the tetragonal phase to the cubic phase and a cation dynamics change with increasing x . However, the Cl/I alloying structures were demonstrated to be unstable over a long term of ~20 days. Time-dependent XRD and solid-state NMR results demonstrated that the Cl atoms gradually dissociated from the Cl/I alloying structures. This Cl dissociation induced a counter transformation from the cubic phase to the tetragonal phase. The photocurrents obtained for photodetectors based on as-synthesized MAPbI_{3-x}Cl_x ($x = 0, 0.05, 0.1, 0.2, \text{ and } 0.3$) absorbers linearly increased with increasing x , but the photocurrents obtained for the same photodetectors after 20 days of storage degraded to photocurrents commensurate with that of MAPbI₃, which supported the results of analyses based on the time-

dependent structural transformations of MAPbI_{3-x}Cl_x single crystals occurring over long time periods. This indicates that the optoelectronic properties of the Cl-doped perovskite materials are strongly correlated with the presence of Cl/I alloying structures. Moreover, the observed long-term instability indicates that different conclusions regarding the effect of Cl ions on the optoelectronic properties of MAPbI_{3-x}Cl_x perovskites may arise over different time scales, which provides a plausible explanation for the long-standing controversy regarding the effect of Cl ions on the performance of optoelectronic devices based on MAPbI_{3-x}Cl_x.

Funding

This work was financially supported by the Ministry of Science and Technology of the People's Republic of China (Grant No. 2018YFC1602800, 2018YFF01012504), the National Natural Science Foundation of China (Grant No. 21574043, 21873028) and Microscale Magnetic Resonance Platform of ECNU.

Author contributions

Y.-F.Y. conceived the project and designed the experiments. W.C.Q. produced the samples. W.C.Q., J.Y., and W.D. fabricated the optoelectronic devices and conducted the device tests. W.C.Q. and O.B. designed the XPS experiments. G. Y., Q.C., W.C.Q., R.H., and Y.-F.Y. analyzed the XRD and NMR experimental data. X.L.W., W.C.Q., and Y.-F.Y. wrote the manuscript. All authors discussed the results and commented on the manuscript.

Data availability

All data needed to evaluate the conclusions in the paper are present in the paper and/or the Supplementary Materials. Additional data related to this paper may be requested from the authors.

Conflict of interest

The authors declare that they have no conflict of interest.

Publisher's note

Springer Nature remains neutral with regard to jurisdictional claims in published maps and institutional affiliations.

Supplementary information is available for this paper at <https://doi.org/10.1038/s41427-020-00249-w>.

Received: 18 April 2020 Revised: 20 July 2020 Accepted: 22 July 2020
Published online: 16 October 2020

References

- Green, M. A., Ho-Baillie, A. & Snaith, H. J. The emergence of perovskite solar cells. *Nat. Photonics* **8**, 506 (2014).
- Park, N.-G. Perovskite solar cells: an emerging photovoltaic technology. *Mater. Today* **18**, 65–72 (2015).
- Jiang, Q. et al. Surface passivation of perovskite film for efficient solar cells. *Nat. Photonics* **13**, 460–466 (2019).
- Dou, L. et al. Solution-processed hybrid perovskite photodetectors with high detectivity. *Nat. Commun.* **5**, 1–6 (2014).
- Lin, K. et al. Perovskite light-emitting diodes with external quantum efficiency exceeding 20 per cent. *Nature* **562**, 245–248 (2018).
- Chin, X. Y., Cortecchia, D., Yin, J., Bruno, A. & Soci, C. Lead iodide perovskite light-emitting field-effect transistor. *Nat. Commun.* **6**, 7383 (2015).
- Zhu, H. et al. Lead halide perovskite nanowire lasers with low lasing thresholds and high quality factors. *Nat. Mater.* **14**, 636–642 (2015).
- Saidaminov, M. I. et al. High-quality bulk hybrid perovskite single crystals within minutes by inverse temperature crystallization. *Nat. Commun.* **6**, 7586 (2015).

9. Dong, Q. et al. Electron-hole diffusion lengths $>175\ \mu\text{m}$ in solution-grown $\text{CH}_3\text{NH}_3\text{PbI}_3$ single crystals. *Science* **347**, 967–970 (2015).
10. Shi, D. et al. Low trap-state density and long carrier diffusion in organolead trihalide perovskite single crystals. *Science* **347**, 519–522 (2015).
11. Tsai, H. et al. Light-induced lattice expansion leads to high-efficiency perovskite solar cells. *Science* **360**, 67–70 (2018).
12. Akkerman, Q. A. et al. Fully inorganic ruddlesden–popper double Cl–I and triple Cl–Br–I lead halide perovskite nanocrystals. *Chem. Mater.* **31**, 2182–2190 (2019).
13. Colella, S. et al. $\text{MAPbI}_3\text{-xCl}$ mixed halide perovskite for hybrid solar cells: the role of chloride as dopant on the transport and structural properties. *Chem. Mater.* **25**, 4613–4618 (2013).
14. Zhang, M. et al. Composition-dependent photoluminescence intensity and prolonged recombination lifetime of perovskite $\text{CH}_3\text{NH}_3\text{PbBr}_3\text{-xCl}$ films. *Chem. Commun.* **50**, 11727–11730 (2014).
15. Wang, Y. et al. Fully ambient-processed mesoscopic semitransparent perovskite solar cells by islands-structure- $\text{MAPbI}_3\text{-xCl}$ -NiO composite and $\text{Al}_2\text{O}_3/\text{NiO}$ interface engineering. *Nano Energy* **49**, 59–66 (2018).
16. Huang, J., Wang, M., Ding, L., Deng, J. & Yao, X. Efficiency enhancement of the $\text{MAPbI}_3\text{-xCl}$ -based perovskite solar cell by a two-step annealing procedure. *Semiconductor Sci. Technol.* **31**, 025009 (2015).
17. Long, M. et al. Large-grain formamidinium $\text{PbI}_3\text{-xBrx}$ for high-performance perovskite solar cells via intermediate halide exchange. *Adv. Energy Mater.* **7**, 1601882 (2017).
18. Heo, J. H., Lee, S.-C., Jung, S.-K., Kwon, O.-P. & Im, S. H. Efficient and thermally stable inverted perovskite solar cells by introduction of non-fullerene electron transporting materials. *J. Mater. Chem. A* **5**, 20615–20622 (2017).
19. Chen, Q. et al. The optoelectronic role of chlorine in $\text{CH}_3\text{NH}_3\text{PbI}_3(\text{Cl})$ -based perovskite solar cells. *Nat. Commun.* **6**, 7269 (2015).
20. Lian, Z. et al. Perovskite $\text{CH}_3\text{NH}_3\text{PbI}_3(\text{Cl})$ single crystals: rapid solution growth, unparalleled crystalline quality, and low trap density toward $10^8\ \text{cm}^{-3}$. *J. Am. Chem. Soc.* **138**, 9409–9412 (2016).
21. Fan, L. et al. Elucidating the role of chlorine in perovskite solar cells. *J. Mater. Chem. A* **5**, 7423–7432 (2017).
22. Zhang, H. et al. Controlled substitution of chlorine for iodine in single-crystal nanofibers of mixed perovskite $\text{MAPbI}_3\text{-xCl}$. *Small* **12**, 3780–3787 (2016).
23. Zhang, C. et al. MAPbCl_3 -mediated decomposition process to tune Cl/PbI₂ distribution in MAPbI_3 films. *ACS Energy Lett.* **3**, 1801–1807 (2018).
24. Min, H. et al. Efficient, stable solar cells by using inherent bandgap of α -phase formamidinium lead iodide. *Science* **366**, 749–753 (2019).
25. Liu, J. & Prezhdo, O. V. Chlorine doping reduces electron–hole recombination in lead iodide perovskites: time-domain ab initio analysis. *J. Phys. Chem. Lett.* **6**, 4463–4469 (2015).
26. Quarti, C., Mosconi, E., Umari, P. & De Angelis, F. Chlorine incorporation in the $\text{CH}_3\text{NH}_3\text{PbI}_3$ perovskite: small concentration, big effect. *Inorg. Chem.* **56**, 74–83 (2017).
27. Saidaminov, M. I. et al. High-quality bulk hybrid perovskite single crystals within minutes by inverse temperature crystallization. *Nat. Commun.* **6**, 1–6 (2015).
28. Liu, Y. et al. Two-inch-sized perovskite $\text{CH}_3\text{NH}_3\text{PbX}_3$ ($\text{X}=\text{Cl}, \text{Br}, \text{I}$) crystals: growth and characterization. *Adv. Mater.* **27**, 5176–5183 (2015).
29. Li, B., Isikgor, F. H., Coskun, H. & Ouyang, J. The effect of methylammonium iodide on the supersaturation and interfacial energy of the crystallization of methylammonium lead triiodide single crystals. *Angew. Chem. Int. Ed.* **56**, 16073–16076 (2017).
30. Baikie, T. et al. Synthesis and crystal chemistry of the hybrid perovskite $(\text{CH}_3\text{NH}_3)\text{PbI}_3$ for solid-state sensitised solar cell applications. *J. Mater. Chem. A* **1**, 5628–5641 (2013).
31. Wang, Q. et al. Transition from the tetragonal to cubic phase of organohalide perovskite: the role of chlorine in crystal formation of $\text{CH}_3\text{NH}_3\text{PbI}_3$ on TiO_2 substrates. *J. Phys. Chem. Lett.* **6**, 4379–4384 (2015).
32. Rosales, B. A. et al. Persistent dopants and phase segregation in organolead mixed-halide perovskites. *Chem. Mater.* **28**, 6848–6859 (2016).
33. Askar, A. M. et al. Composition-tunable formamidinium lead mixed halide perovskites via solvent-free mechanochemical synthesis: decoding the Pb environments using solid-state NMR spectroscopy. *J. Phys. Chem. Lett.* **9**, 2671–2677 (2018).
34. Bernard, G. M. et al. Methylammonium cation dynamics in methylammonium lead halide perovskites: a solid-state NMR perspective. *J. Phys. Chem. A* **122**, 1560–1573 (2018).
35. Fabini, D. H. et al. Universal dynamics of molecular reorientation in hybrid lead iodide perovskites. *J. Am. Chem. Soc.* **139**, 16875–16884 (2017).
36. Wang, J. et al. A small lattice change induces significant dynamic changes of CH_3NH_3^+ caged in hybrid perovskite crystals: toward understanding the interplay between host lattices and guest molecules. *Inorg. Chem.* **58**, 7426–7432 (2019).
37. Franssen, W. M., van Es, S. G., Dervišođlu, R., de Wijs, G. A. & Kentgens, A. P. Symmetry, dynamics, and defects in methylammonium lead halide perovskites. *J. Phys. Chem. Lett.* **8**, 61–66 (2017).
38. Kubicki, D. J. et al. Cation dynamics in mixed-cation $(\text{MA})_x(\text{FA})_{1-x}\text{PbI}_3$ hybrid perovskites from solid-state NMR. *J. Am. Chem. Soc.* **139**, 10055–10061 (2017).
39. Kim, M. et al. Methylammonium chloride induces intermediate phase stabilization for efficient perovskite solar cells. *Joule* **3**, 2179–2192 (2019).
40. Walsh, A., Scanlon, D. O., Chen, S., Gong, X. & Wei, S. H. Self-regulation mechanism for charged point defects in hybrid halide perovskites. *Angew. Chem. Int. Ed.* **54**, 1791–1794 (2015).
41. Christians, J. A., Habisreutinger, S. N., Berry, J. J. & Luther, J. M. Stability in perovskite photovoltaics: a paradigm for newfangled technologies. *ACS Energy Lett.* **3**, 2136–2143 (2018).
42. Brennan, M. C. et al. Superlattices are greener on the other side: how light transforms self-assembled mixed halide perovskite nanocrystals. *ACS Energy Lett.* **5**, 1465–1473 (2020).
43. Brennan, M. C., Ruth, A., Kamat, P. V. & Kuno, M. Photoinduced anion segregation in mixed halide perovskites. *Trends Chem.* **2**, <https://doi.org/10.1016/j.trechm.2020.01.010> (2020).
44. Draguta, S. et al. Rationalizing the light-induced phase separation of mixed halide organic–inorganic perovskites. *Nat. Commun.* **8**, 1–8 (2017).